



Ground-based measurements of airborne Saharan dust in marine environment during the NAMMA field experiment

Myeong-Jae Jeong,^{1,2} Si-Chee Tsay,² Qiang Ji,^{2,3} N. Christina Hsu,² Richard A. Hansell,^{2,3} and Joonsuk Lee^{2,3}

Received 5 August 2008; accepted 15 September 2008; published 17 October 2008.

[1] Several episodes of airborne mineral dust transported from the Saharan deserts were observed at Sal Island, Cape Verde for 2–28 September 2006 during the NASA African Monsoon Multidisciplinary Analyses (NAMMA) field experiment. Dust particles were mixed with marine background aerosols when the dust layers descended into the marine boundary layer. A new method is developed to derive the optical properties of dust when mixed with maritime aerosols. The derived single scattering albedo and mass scattering efficiency differed significantly between two selected cases leading to differences in their direct radiative effects. Back-trajectory analyses suggest that the two cases were influenced by dust particles originating from different source regions over North Africa. This stresses the importance of resolving dust optical properties in sub-regional scales to attain a better assessment of the role of airborne dust on the climate system. **Citation:** Jeong, M.-J., S.-C. Tsay, Q. Ji, N. C. Hsu, R. A. Hansell, and J. Lee (2008), Ground-based measurements of airborne Saharan dust in marine environment during the NAMMA field experiment, *Geophys. Res. Lett.*, 35, L20805, doi:10.1029/2008GL035587.

1. Introduction

[2] Airborne Saharan dust (ASD) is the most important source of airborne mineral dust nearly year-round [*Ginoux et al.*, 2001; *Prospero and Lamb*, 2003], rendering large radiative effects [*Teegen et al.*, 1997], while its impact on the climate system still poses significant uncertainty [*Forster et al.*, 2007]. Characterizing the optical properties of ASD together with its spatial distribution is crucial, as these factors can introduce differential heating/cooling in the atmosphere and surface, thereby causing abrupt changes in the atmospheric circulation [e.g., *Lau et al.*, 2006]. There have been many field experiments to measure the optical properties of Saharan dust [e.g., *Reid and Maring*, 2003; *Tanré et al.*, 2003]. National Aeronautics and Space Administration (NASA)'s African Monsoon Multidisciplinary Analyses (NAMMA) is the latest effort to remedy the lack of comprehensive observations in the West African region. Most observations of NAMMA are air-borne measurements; however, these can be exceedingly difficult to make from fast moving aircrafts, particularly for large-

sized dust particles. Although measurement systems can be more effectively controlled using ground-based instruments to attain optimum conditions for measuring coarse-mode dust, there are still inherent difficulties in dust measurements. One of the obstacles is that the dust layers have to reach the surface, and even when they do, the dust particles get mixed with aerosols in the marine boundary layer (MBL). Thus, normally, much more expensive instruments like mass spectrometers or laborious chemical analyses have been needed to acquire the dust optical properties from the surface measurements.

[3] In this paper, a new method to separate the properties of airborne dust from those of the marine background aerosols using popular and relatively inexpensive instrumentation is described. The method allows for the dry mass concentration, mass scattering efficiency (MSE) and single scattering albedo (SSA) of dust to be estimated. Two dust episodes are contrasted to highlight the importance of resolving dust optical properties to assess their radiative effects more accurately.

2. Measurements

[4] Intensive measurements of aerosols, clouds, and radiation were made by the NASA's Surface-sensing Measurements for Atmospheric Radiative Transfer (SMART) and Chemical, Optical, and Microphysical Measurements of in situ Troposphere (COMMIT) mobile laboratories as part of a contributing effort during the NAMMA field experiment held at Sal island, Cape Verde (Aug–Sep, 2006). SMART carries a suite of radiometric sensors for measuring fluxes and radiances over a wide spectral range spanning wavelengths from the ultraviolet to the microwave and a Micro-Pulse Lidar (MPL) monitoring the vertical profiles of aerosols and clouds. COMMIT is equipped with (1) a three-wavelength (450, 550, and 700 nm) nephelometer (TSI), (2) three single-wavelength (530 nm) nephelometers (Radiance Research) with variable relative humidity (RH) settings (~40%, ambient, and ~85%), (3) a three-wavelength (467, 530, and 660 nm) Particle/Soot Absorption Photometer (PSAP; Radiance Research), (4) a TEOM aerosol mass concentration monitor (Thermo Electron Corp.), (5) an Aerodynamic Particle Sizer (APS; TSI), (6) CO₂, CO, NO_x, SO₂, and O₃ gas monitors (Thermo Electron Corp.) and some more. Systematic data reduction procedures established for the COMMIT system were applied to these in situ data. Details of the complete instrumentation for SMART-COMMIT are provided at <http://smart-commit.gsfc.nasa.gov/>.

[5] After considering the inlets and tubing for individual instruments [*Baron and Willeke*, 2001] in COMMIT, the derived sampling efficiencies together with APS-derived

¹Goddard Earth Sciences and Technology Center, University of Maryland Baltimore County, Baltimore, Maryland, USA.

²NASA Goddard Space Flight Center, Greenbelt, Maryland, USA.

³Earth System Science Interdisciplinary Center, University of Maryland, College Park, Maryland, USA.

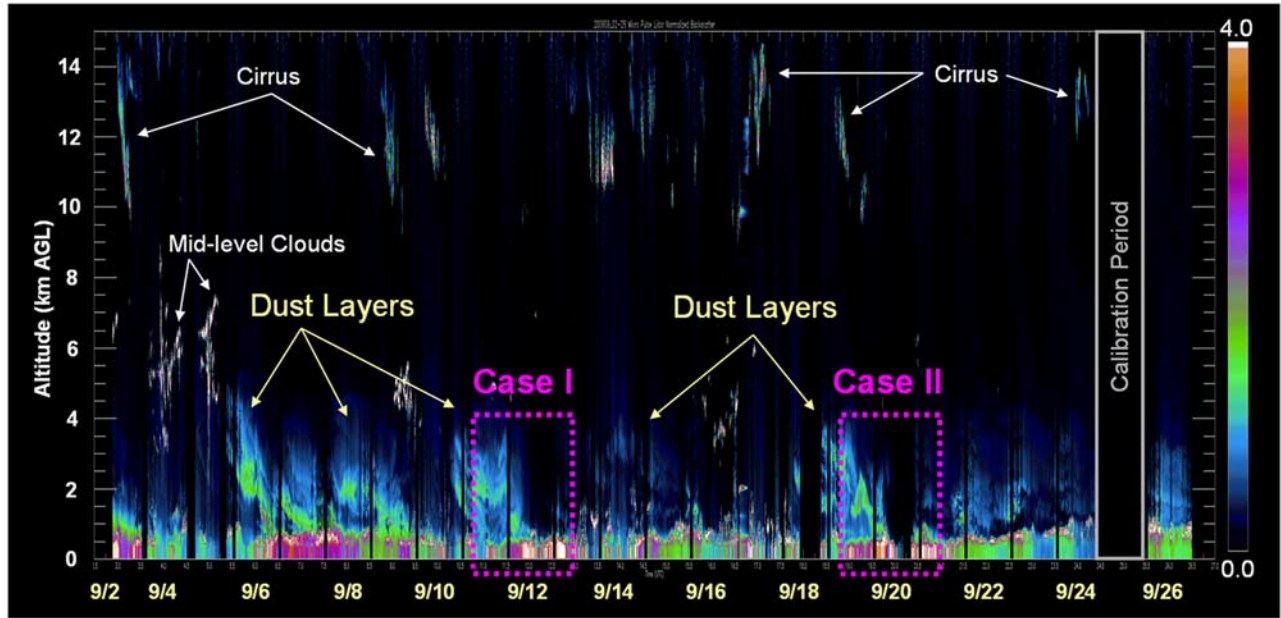


Figure 1. Time series of normalized back-scatter profiles measured from Micro-Pulse Lidar (MPL) at Sal, Cape Verde during 2–26 Sep 2006. Dust layers are seen in green and light blue around 1–4 km above the ground level (AGL). The two dust episodes investigated in this study are outlined by pink boxes. Cirrus clouds (10–15 km AGL) associated with large-scale atmospheric circulation were frequently observed during the field experiment.

aerosol size distributions were used to ensure all the instruments could measure the equivalent aerosol mass. In general, a loss of particles is expected due to imperfect, but inevitable, sampling inefficiency. For example, for particles with diameter less than 10 μm (PM10), the TEOM, TSI nephelometer, and PSAP experienced mass losses of 2.8%, 2.9%, and 14.7%, respectively during the dust episodes to be discussed in this study. This differential mass loss among instruments can lead to errors in the derived quantities such as aerosol MSE and SSA. The current assessment on the reductions in the scattering and absorption coefficients (at 550 nm) due to the corresponding mass losses are 1.4% and 11.9%, respectively. Additionally, conventional correction methods [Anderson and Ogren, 1998; Bond et al., 1999] suggested for the TSI nephelometer and PSAP measurements were applied accordingly.

[6] In this study, scattering and absorption coefficients from the TSI nephelometer and PSAP, and TEOM mass concentration were used to derive SSA and MSE. Aerosol humidification factor (AHF), defined as the ratio of the aerosol scattering coefficient at $\text{RH} = 85\%$ to that at $\text{RH} = 40\%$ was calculated at 530 nm using the same method adopted by Jeong et al. [2007] and regarded as the values at 550 nm. All the in situ measured aerosol parameters are defined for PM10 (diameter equal to or less than 10 μm) unless specifically mentioned otherwise.

[7] Sal (16.7N, 22.9W), Cape Verde is a small island ($\sim 216 \text{ km}^2$) located about 640 kilometers off the coast of northwestern Africa. Surrounded by an open ocean, maritime aerosols are dominant year-round unless Saharan dust passes over the island. During the SMART-COMMIT deployment, several dust episodes were captured, in which the dust layers descended into the MBL, so that optical properties of dust mixed with the MBL aerosols could be

measured in situ at the surface (Figure 1). In this study, we focus on two of such cases – Case-I for the Sep 11–13 and Case-II for Sep 19–20.

3. Derivation of Dust Optical Properties

[8] During the deployment, aerosol precursor trace gases such as CO , SO_2 , NO_x , and O_3 were monitored simultaneously. The data indicated there were no significant influences of local pollution during the entire experiment period. This allows us to assume that the changes in aerosol properties at Sal are associated with transported dust. Exploiting this unique opportunity, a new method to derive the dust optical properties from those of aerosol mixtures is described below.

[9] Suppose that a volume of aerosol samples is a mixture of two components, namely “dust” and “background” aerosols. The measured aerosol scattering coefficients become the sum of the two components:

$$k_{sca,Mix}(\text{RH}) = k_{sca,Bg}(\text{RH}) + k_{sca,Du}(\text{RH}), \quad (1)$$

where $k_{sca,Mix}(\text{RH})$, $k_{sca,Bg}(\text{RH})$, and $k_{sca,Du}(\text{RH})$ denote the scattering coefficients for an aerosol mixture (or a volume of aerosols being actually measured), marine background aerosols, and dust at a given relative humidity (RH), respectively. Hereinafter, the subscripts, “Mix”, “Bg”, and “Du”, will denote the aerosol parameters for mixture, background, and dust, respectively. A MSE, $\sigma_{sca}(\text{RH})$, for aerosols is defined by the ratio of the scattering coefficient to the dry aerosol mass concentration (M_{Mix}^d):

$$\sigma_{sca,Mix}(\text{RH}) = k_{sca,Mix}(\text{RH})/M_{Mix}^d. \quad (2)$$

From equations (1) and (2), the MSE can be broken down into the sum of the two aerosol components; i.e.,

$$\sigma_{sca,Mix}(RH) = (1 - w_{Du})\sigma_{sca,Bg}(RH) + w_{Du}\sigma_{sca,Du}(RH), \quad (3)$$

where $w_{Du} = M_{Du}^d / (M_{Bg}^d + M_{Du}^d)$. AHF at a RH value of interest, $f(RH)$, is defined as follows:

$$f(RH) \equiv k_{sca}(RH\%) / k_{sca}(40\%). \quad (4)$$

$f(RH)$ with $RH = 85\%$ [i.e., $f(85\%)$] is often used as an indicator of hygroscopicity of aerosols. By combining equations (1) and (4), $f(85\%)$ for an aerosol mixture can be written as:

$$f_{Mix}(85\%) = \frac{k_{sca,Mix}(85\%)}{k_{sca,Mix}(40\%)} \approx \frac{k_{sca,Bg}(85\%) + k_{sca,Du}(85\%)}{k_{sca,Bg}(40\%) + k_{sca,Du}(40\%)}. \quad (5)$$

For brevity of equations, a parameter, γ , is defined as

$$\gamma \equiv \frac{k_{sca,Du}(40\%)}{k_{sca,Bg}(40\%)} = \frac{f_{Bg}(85\%) - f_{Mix}(85\%)}{f_{Mix}(85\%) - f_{Du}(85\%)}. \quad (6)$$

Manipulations lead to the following relationships between the scattering coefficients for dust (background) aerosols and an aerosol mixture:

$$k_{sca,Du}(40\%) \equiv \frac{\gamma}{\gamma + 1} k_{sca,Mix}(40\%);$$

$$k_{sca,Bg}(40\%) \equiv \frac{1}{\gamma + 1} k_{sca,Mix}(40\%). \quad (7)$$

By combining equations (2) and (7), relationships between aerosol mass concentration and aerosol scattering coefficients for the respective aerosol components are derived as follows:

$$M_{Bg}^d = \frac{k_{sca,Mix}(40\%)}{\sigma_{sca,Bg}(40\%) \cdot (\gamma + 1)};$$

$$M_{Du}^d = M_{Mix}^d - \frac{k_{sca,Mix}(40\%)}{\sigma_{sca,Bg}(40\%) \cdot (\gamma + 1)}. \quad (8)$$

Thus, MSE for dust becomes

$$\sigma_{sca,Du} = \frac{\gamma}{M_{Du}^d(\gamma + 1)} k_{sca,Mix}(40\%). \quad (9)$$

SSA for an aerosol mixture can be written as

$$\omega_{Mix} = \frac{k_{sca,Bg}(40\%) + k_{sca,Du}(40\%)}{k_{sca,Bg}(40\%) + k_{sca,Du}(40\%) + k_{abs,Bg}(40\%) + k_{abs,Du}(40\%)}. \quad (10)$$

Finally, combining equations (6) and (10) results in a relationship among SSAs for dust, background aerosols, and an aerosol mixture:

$$\omega_{Du} = [(1 + \gamma)\omega_{Mix} - \omega_{Bg}] / \gamma. \quad (11)$$

4. Results of in Situ Measurements

[10] In order to derive dust optical properties using the equations in section 3, the following parameters need to be considered as *a priori*: (1) “Background” MSE [$\sigma_{sca,Bg}$], (2) “Background” $f(85\%)$ [$f_{Bg}(85\%)$], (3) “Background” SSA [ω_{Bg}], and (4) “Dust” $f(85\%)$ [$f_{Du}(85\%)$]. Thus,

“Background” conditions are determined by examining the time series of all available measurements during the experiment. Relatively lower scattering and absorption coefficients and higher $f(85\%)$ were found between dust episodes and averages for such conditions are considered as the ones for background. The averages (± 1 Std.) of $\sigma_{sca,Bg}$, $f_{Bg}(85\%)$, and ω_{Bg} are $1.54 (\pm 0.19) \text{ m}^2 \text{ g}^{-1}$, $2.50 (\pm 0.05)$, and $0.995 (\pm 0.005)$ at 550 nm, respectively. The values for $f_{Du}(85\%)$ is assumed to be 1.1 [Anderson *et al.*, 2003]. Unless specifically mentioned, the optical properties at 550 nm will be derived in this study since $f(85\%)$ measurements were available only at 550 nm.

[11] The dust optical properties for cases I and II are derived using the set of equations (equations (1)–(11)) with these *a priori* values. Figure 2 shows measured and derived quantities of aerosols for these two cases. The peaks in the measured scattering coefficients and aerosol mass concentrations are primarily due to dust while those for the background aerosols remain relatively constant. The averages and standard deviations for the dust optical properties are provided in Table 1. A minimum threshold of 30 Mm^{-1} for the scattering coefficient was set for the statistics in order to remove noisy data associated with low signals. The results are within the ranges that can be found in the literature [e.g., Hand and Malm, 2007].

[12] Sensitivity tests carried out for the derived dust optical properties (see Figures S1 and S2 and Tables S1 and S2, referred to in Text S1 of the auxiliary material) showed that uncertainties ($\sim \pm 10\%$) in *a priori* parameters can result in errors of 10–15% and less than 3%, respectively for the dust MSE and dust SSA.¹ An additional uncertainty in the derived dust MSE might exist due to possible loss of volatile aerosol mass by the TEOM instrument [e.g., Kingham *et al.*, 2006]. Unfortunately, there was no information on the contributions of volatile aerosols to the total aerosol mass during the field experiment. Although it is anticipated that the effect of “missing” mass of volatile aerosols on the derived dust MSE in this study would not be so large as reported for smoke aerosols (e.g., $\sim 28\%$ from Kingham *et al.* [2006]), it clearly warrants future investigations about such effects of volatile aerosols on dust measurements. Nevertheless, interestingly enough, the derived dust optical properties for the two cases are quite different from each other (see Table 1). Possible explanations and relevant discussions are provided in section 5.

5. Investigation of Dust Source Regions

[13] As illustrated in section 4, the dust optical properties for the two cases showed large differences. Especially, ω_{Du} for the two cases differed by more than 0.05, exceeding the ranges of uncertainties due to errors in the *a priori* parameters (Figure S2). Many factors may be at play, such as (1) differences in the dust size distributions due to a size-differential deposition, and (2) differences in the chemical compositions for the two cases. Aerosol size measurements from the APS for Case-II and some other dust episodes during the field experiments showed the same patterns of increases in particle number concentrations for the diameter

¹Auxiliary materials are available in the HTML. doi:10.1029/2008GL035587.

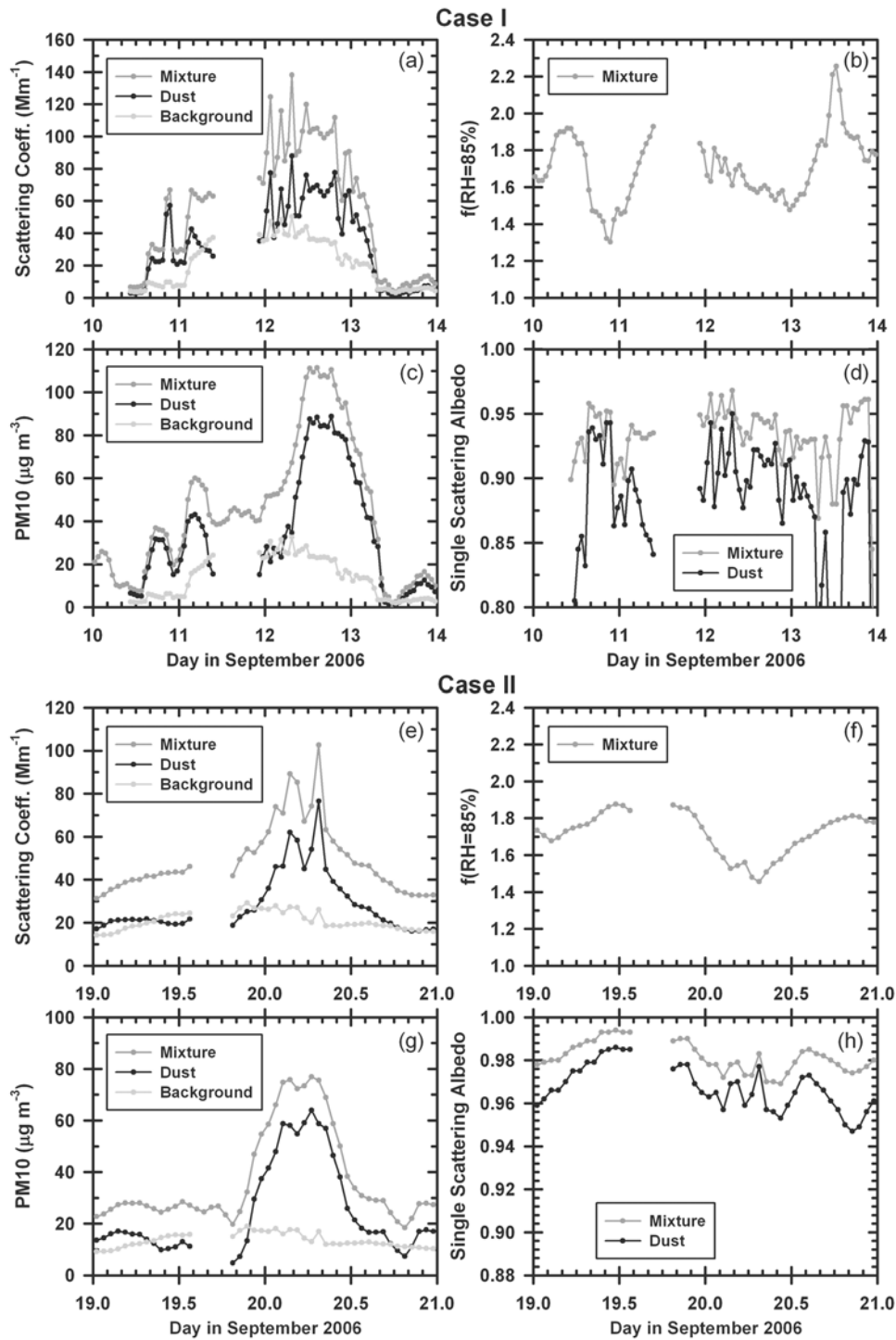


Figure 2. (a–d) Scattering coefficients, $f(85\%)$, mass concentration, and SSA for Mixture, Background, and Dust aerosols during 10–13 Sep. (e–h) Same as Figures 2a–2d, but during 19–20 Sep. All the aerosol parameters are defined for particles with diameter equal to or less than $10\mu\text{m}$. The reference wavelength and RH for scattering coefficients, $f(85\%)$ and SSA are 550 nm and 40% , respectively.

ranges between 0.8 and $2\mu\text{m}$, which suggests that size distributions may not be a major factor. Therefore we assume that different chemical composition is a more likely explanation. For example, the iron content of the mineral dust in the form of hematite is an efficient light absorber in the visible [Sokolik and Toon, 1999]. In addition, various types and contents of clays, quartz, fragmented fossil

Table 1. Mean and Standard Deviation of the Derived Dust Mass Scattering Efficiency and Dust Single Scattering Albedo

	Parameter	Mean (\pm SD)
Case-I	$\sigma_{sca,Du}(40\%) [\text{m}^2 \text{g}^{-1}]$	1.21 (\pm 0.71)
	$\omega_{Du} (0.55\mu\text{m})$	0.900 (\pm 0.049)
Case-II	$\sigma_{sca,Du} (40\%) [\text{m}^2 \text{g}^{-1}]$	0.93 (\pm 0.17)
	$\omega_{Du} (0.55\mu\text{m})$	0.961 (\pm 0.012)

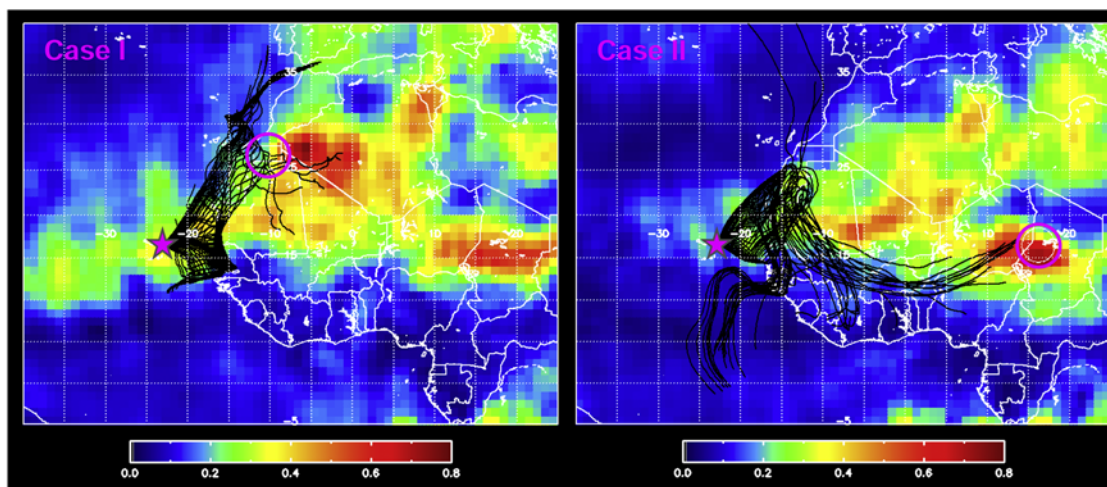


Figure 3. MODIS AOT (550 nm) averaged for 7 days on and prior to the beginning of each case. Superimposed black lines are 7-day back-trajectories terminating at Sal (16.7N, 22.9W; star symbols). Each line represents a back-trajectory ending at every hour throughout the period of each case. Pink circles stand for the estimated source regions for dust observed at Sal each case.

diatoms introduce wide ranges of spectrally differential absorption [Sokolik and Toon, 1999; Todd et al., 2007], which could explain the different ω_{Du} for both cases. Since such contents of mineral components depend on the soil properties of the source regions, it is necessary to find out where the dust for the two cases originated.

[14] In order to locate possible pathways of the dust, back-trajectories with duration of 7 days and end-point at Sal island were calculated every hour using the HYSPLIT model (R. R. Draxler and G. D. Rolph, HYSPLIT model, 2003, available at <http://www.arl.noaa.gov/ready/hysplit4.html>), during the periods of dust episodes for cases I and II. Figure 3 shows the resultant back-trajectories for the two cases superimposed with 7-day averages of AOT (550 nm) from the composites of the operational MODerate resolution Imaging Spectrometer (MODIS) *Deep Blue* (over the Saharan desert) [Hsu et al., 2004] and *Dark Target* aerosol products (over ocean and vegetated land) [Remer et al., 2005]. In Figure 3, the areas with high AOT indicate the location and loading of dust during the respective periods. This was cross-checked with the UV Aerosol Index (AI) from the Ozone Monitoring Instrument aboard the Aura satellite. UV AI has been widely used to detect dust and biomass burning smoke [e.g., Hsu et al., 1999; Jeong and Li, 2005]. The areas of high AOT over the Sahara are considered to be possible source regions, especially those crossed by back-trajectories. To make sure, we searched for areas with sudden incidences of enhanced AOT and UV AI on a certain day compared to the previous day around the crosses between the back-trajectories and areas of the enhanced AOT and UV AI. The corresponding areas are marked in the Figure 3 by pink circles. We believe that these areas may have been significant sources contributing to the observed dust for the respective cases. The results indicate that the dust measured at the surface of Sal originate from different source regions between the two cases.

[15] MODIS *Deep Blue* (DB) aerosol products operationally reports AOT over bright surfaces and SSA (at 412 nm) for dust pixels (hereinafter, DB SSA). ω_{Du} derived in this

study is compared with DB SSA. DB SSA over the estimated source regions (pink circles in Figure 3) were averaged for dust pixels (with AOT > 1.0) for the respective cases. As a result, DB SSA for cases I and II are 0.915 (Std = 0.004; AOT = 1.381 ± 0.270), 0.959 (Std = 0.011; AOT = 2.833 ± 0.769), respectively. Direct comparison may not be appropriate due to discrepancies in wavelengths and target aerosol volumes. However, DB SSA over the two locations in North Africa is consistent with the ω_{Du} derived from surface measurements, supporting the possibility that the two locations are the source regions for the two cases.

6. Discussion and Conclusion

[16] The values of SSA between the two cases, which possibly represent dust originating from different source regions in North Africa, are significantly different. Our assessment (see Text S2) suggests that the dust for the two cases could yield 10.1 Wm^{-2} and -18.7 Wm^{-2} of differences in daily mean direct radiative effects for a visible band (400–700 nm) at the TOA and the surface, respectively (Case-I minus Case-II; AOT at 550 nm was assumed to be unity). Atmospheric absorption due to the presence of dust could differ by 28.8 Wm^{-2} between the two cases under the same conditions. Such differences in absorption could lead to significant uncertainty in assessments of the regional energy budget unless dust optical properties are properly resolved. Dust size distributions are taken into account by some leading aerosol transport models and climate models [e.g., Ginoux et al., 2001; Zender et al., 2003], but their optical properties are generally fixed over the globe. Given the wide ranges of dust optical properties – even larger than the differences between the two cases of this study – adopted by various climate models [Kinne et al., 2006; Hand and Malm, 2007], significant discrepancies in the radiative absorption are expected among various models, thereby introducing different heating/cooling rates of the atmosphere and surface. This in turn can cause changes in atmospheric circulation. Therefore, it may be considered

necessary for aerosol transport/climate models to resolve dust optical properties depending on source regions or mineralogy in order to reduce uncertainties in the impact of airborne mineral dust on regional and global climate systems.

[17] **Acknowledgments.** We gratefully acknowledge the NOAA Air Resources Laboratory (ARL) for the provision of the HYSPLIT transport and dispersion model and READY website (<http://www.arl.noaa.gov/ready.html>) used in this publication. This research was funded by NASA grant NNX06AE10G, managed by H. Maring.

References

- Anderson, T. L., and J. A. Ogren (1998), Determining aerosol radiative properties using the TSI 3563 integrating nephelometer, *Aerosol Sci. Technol.*, *29*, 57–69.
- Anderson, T. L., S. J. Masonis, D. S. Covert, N. C. Ahlquist, S. G. Howell, A. D. Clarke, and C. S. McNaughton (2003), Variability of aerosol optical properties derived from in situ aircraft measurements during ACE-Asia, *J. Geophys. Res.*, *108*(D23), 8647, doi:10.1029/2002JD003247.
- Baron, P. A., and K. Willeke (Eds.) (2001), *Aerosol Measurement: Principles, Techniques, and Applications*, 2nd ed., 1131 pp., Wiley-Interscience, New York.
- Bond, T. C., T. L. Anderson, and D. Campbell (1999), Calibration and intercomparison of filter-based measurements of visible light absorption by aerosols, *Aerosol Sci. Technol.*, *30*, 582–600.
- Forster, P., et al. (2007), Changes in atmospheric constituents and in radiative forcing, in *Climate Change 2007: The Physical Science Basis. Contribution of Working Group I to the Fourth Assessment Report of the Intergovernmental Panel on Climate Change*, edited by S. Solomon et al., pp. 129–234, Cambridge Univ. Press, Cambridge, U. K.
- Ginoux, P., M. Chin, I. Tegen, J. M. Prospero, B. Holben, O. Dubovik, and S.-J. Lin (2001), Sources and distributions of dust aerosols simulated with the GOCART model, *J. Geophys. Res.*, *106*, 20,255–20,273.
- Hand, J. L., and W. C. Malm (2007), Review of aerosol mass scattering efficiencies from ground-based measurements since 1990, *J. Geophys. Res.*, *112*, D16203, doi:10.1029/2007JD008484.
- Hsu, N. C., J. R. Herman, O. Torres, B. N. Holben, D. Tanre, T. F. Eck, A. Smirnov, B. Chatenet, and F. Lavenu (1999), Comparisons of the TOMS aerosol index with Sun-photometer aerosol optical thickness: Results and applications, *J. Geophys. Res.*, *104*, 6269–6279.
- Hsu, N. C., et al. (2004), Aerosol properties over bright-reflecting source regions, *IEEE Trans. Geosci. Remote Sens.*, *42*, 557–569.
- Jeong, M.-J., and Z. Li (2005), Quality, compatibility, and synergy analyses of global aerosol products derived from the advanced very high resolution radiometer and Total Ozone Mapping Spectrometer, *J. Geophys. Res.*, *110*, D10S08, doi:10.1029/2004JD004647.
- Jeong, M.-J., Z. Li, E. Andrews, and S.-C. Tsay (2007), Effect of aerosol humidification on the column aerosol optical thickness over the Atmospheric Radiation Measurement Southern Great Plains site, *J. Geophys. Res.*, *112*, D10202, doi:10.1029/2006JD007176.
- Kingham, S., et al. (2006), Winter comparison of TEOM, MiniVol and DustTrak PM10 monitors in a woodsmoke environment, *Atmos. Environ.*, *40*, 338–347.
- Kinne, S., et al. (2006), An AeroCom initial assessment—Optical properties in aerosol component modules of global models, *Atmos. Chem. Phys.*, *6*, 1815–1834.
- Lau, K. M., et al. (2006), Asian monsoon anomalies induced by aerosol direct effects, *Clim. Dyn.*, *26*, 855–864, doi:10.1007/s00382-006-0114-z.
- Prospero, J. M., and P. J. Lamb (2003), African droughts and dust transport to the Caribbean: Climate change implications, *Science*, *302*, 1024–1027.
- Reid, J. S., and H. B. Maring (2003), Foreword to special section on the Puerto Rico Dust Experiment (PRIDE), *J. Geophys. Res.*, *108*(D19), 8585, doi:10.1029/2003JD003510.
- Remer, L. A., et al. (2005), The MODIS aerosol algorithm, products, and validation, *J. Atmos. Sci.*, *62*, 947–973.
- Sokolik, I. N., and O. B. Toon (1999), Incorporation of mineralogical composition into models of the radiative properties of mineral aerosol from UV to IR wavelengths, *J. Geophys. Res.*, *104*, 9423–9444.
- Tanré, D., J. Haywood, J. Pelon, J. F. Léon, B. Chatenet, P. Formenti, P. Francis, P. Goloub, E. J. Highwood, and G. Myhre (2003), Measurement and modeling of the Saharan dust radiative impact: Overview of the Saharan Dust Experiment (SHADE), *J. Geophys. Res.*, *108*(D18), 8574, doi:10.1029/2002JD003273.
- Tegen, I., P. Hollrig, M. Chin, I. Fung, D. Jacob, and J. Penner (1997), Contribution of different aerosol species to the global aerosol extinction optical thickness: Estimates from model results, *J. Geophys. Res.*, *102*, 23,895–23,915.
- Todd, M. C., R. Washington, J. V. Martins, O. Dubovik, G. Lizcano, S. M'Bainayel, and S. Engelstaedter (2007), Mineral dust emission from the Bodélé Depression, northern Chad, during BoDEx 2005, *J. Geophys. Res.*, *112*, D06207, doi:10.1029/2006JD007170.
- Zender, C. S., H. Bian, and D. Newman (2003), Mineral Dust Entrainment and Deposition (DEAD) model: Description and 1990s dust climatology, *J. Geophys. Res.*, *108*(D14), 4416, doi:10.1029/2002JD002775.

R. A. Hansell, N. C. Hsu, Q. Ji, J. Lee, and S.-C. Tsay, Laboratory for Atmospheres, NASA Goddard Space Flight Center, Code 613.2, Greenbelt, MD 20771, USA.

M.-J. Jeong, Goddard Earth Sciences and Technology Center, University of Maryland Baltimore County, 5523 Research Park Drive, Suite 320, Baltimore, MD 21228, USA. (myeong-jae.jeong-1@nasa.gov)